An ultrasonic and thermal expansion study of the quasi-one-dimensional compound $(TaSe_4)_2I$

1996 J. Phys.: Condens. Matter 8 2021

(http://iopscience.iop.org/0953-8984/8/12/015)

J. Phys.: Condens. Matter **8** (1996) 2021–2041. Printed in the UK

An ultrasonic and thermal expansion study of the quasi-one-dimensional compound $(TaSe_4)_2I$

M Saint-Paul†, S Holtmeier†‖, R Britel†, P Monceau†, R Currat‡ and F Levy§

† Centre de Recherches sur les Très Basses Températures, associé à l'Université Joseph Fourier, CNRS, BP 166, 38042 Grenoble Cédex 9, France

‡ Institut Laue–Langevin, BP 166, 38042 Grenoble Cédex 9, France

§ Institut de Physique Appliquée, Ecole Polytechnique de Lausanne, CH-1015 Lausanne, Switzerland

Received 15 November 1995

Abstract. We report ultrasonic and thermal expansion measurements on quasi-one-dimensional $(TaSe_4)_2I$. The elastic constant C_{44} exhibits strong anomalies over a wide temperature range around the Peierls transition. Anisotropic behaviour of the slow shear mode C_{44} propagating along and perpendicular to the chain direction is observed around T_P. Elastic constants, like electrical resistance, are very sensitive to a small Nb content substituted for Ta. Anomalous behaviour of C_{44} at low temperatures is reported. We also present measurements of the anisotropic thermal expansion coefficients.

1. Introduction

One-dimensional metallic compounds have been shown to be unstable towards the formation of a semiconductor called a Peierls insulator. This instability is characterized by the opening of a gap in the electronic spectrum at the Fermi level $2k_F$ and by a lattice distortion. In one-dimensional systems a lattice distortion with a wavelength $2\pi/2k_F$ will lower the electronic energy more than the elastic energy cost of the ionic distortion. The Peierls instability has attracted much interest [1] in the last few years because chemists have been able to synthesize inorganic as well as organic one-dimensional materials which exhibit the Peierls phase transition, namely transition metal trichalcogenides $NbSe_3$, TaS_3, ..., molybdenum oxides such as $K_{0.3}MoO_3$, and quasi-one-dimensional halogenated metal tetrachalcogenides $(MSe_4)I$ with M = Ta, Nb. These latter compounds consist of (MSe_4) chains parallel to the crystallographic ***c***-axis well separated from one another by iodine strands [2]. In each MSe_4 chain the metal atom is located at the centre of a rectangular antiprism of eight Se atoms. The band filling of the d_{z^2} transition metal M can be varied by varying the composition [3]. This change in band filling leads to quite different structural and electrical properties [2, 3]. $(TaSe_4)_2I$ undergoes a Peierls transition at $T_P = 263$ K [4, 5]. This transition involves the formation of a charge-density wave (CDW) with an associated periodic lattice distortion. Superlattice reflections have been observed in the incommensurate CDW phase by electron diffraction [6], x-rays [7, 8] and neutron [9, 10] experiments. From the satellite extension rules it was found that the atomic displacements were transverse, acoustic-like

‖ Present address: Physikalisches Institut, Goethe Universität, Frankfurt, Germany.

0953-8984/96/122021+21$19.50

and predominantly polarized in the basal plane along [1$\bar{1}$0] [7, 8]. Inelastic neutron spectra show little evidence [10] for a soft-mode instability at T_P. The critical dynamics associated with the Peierls transition appears to be primarily of the slow relaxational type (with an unresolved central peak). No softening of any of the lower-frequency optic modes has been detected [10], contrarily to the interphonon transverse acoustic–transverse optic interaction model initially proposed by Sugai *et al* [11]. Softening of the Young modulus by the vibrating-reed technique [12] and of the torsion modulus [13] at very low frequencies has been observed in this system, which is a general feature of the CDW phase transition. Few experimental investigations with ultrasonic methods have been reported so far [14].

The incommensurate CDW transition is a second-order one, and thermodynamic anomalies are expected to be related to the Ehrenfest relations. The CDW causes the onset of three-dimensional order with large fluctuations of the order parameter occurring above T_P [1]. Softening of the Young modulus has been analysed in two other quasi-one-dimensional compounds (TaS_3 and $K_{0.3}MoO_3$) using the three-dimensional XY-model [21].

Hereafter we present an intensive study of the elastic constants of pure and Nb-doped $(TaSe_4)_2I$ single crystals using the ultrasound technique. A sharp softening of the shear elastic constant C_{44} is measured at T_P. The dispersion of C_{44} propagating parallel and perpendicular to the chain axis exhibits a strongly anisotropic behaviour. Measurements of the thermal expansion have also been made on the same samples and are reported.

The paper is organized as follows: in the second section we briefly describe the experimental technique. The experimental results are reported in the third section. In the fourth section we first describe the expectation of the elastic anomaly at T_P in the mean-field approximation. The analysis of the data leads to the evolution of the critical exponents of the elastic constants and of the thermal expansion. Finally an anisotropic process and electro-acoustic effects are reported.

2. Experiment

We have made measurements for several samples from several batches: A, B and C for pure $(TaSe_4)_2I$, D for doped crystals with a nominal concentration of 0.2% Nb, E for doped crystals with a nominal concentration of 1.2% Nb. Electrical resistance measurements on crystals in different batches allowed us to determine the Peierls transition temperature T_P. This temperature is better defined at the peak of the logarithmic derivative of R versus temperature as shown in figure 1. The width of the peak gives an indication of the purity of the sample. It is seen that doping smears out the phase transition. T_P is respectively 263 K, 250 K and 245 K for batches A, B, C. A similar variation in T_P has often been observed by other groups and is presumably due to a non-stoichiometry of the iodine content. T_P for batch D is 246 K and that for batch E is not well defined but is around 200 K.

The crystals used for ultrasound measurements have typical dimensions of $4\times3\times3$ mm^3; the largest dimension is parallel to the $\boldsymbol{c}$-axis [001] direction. Parallel faces were cut perpendicularly to the [001] direction. Samples having faces of good quality (mirror like) were used as received to generate longitudinal and shear elastic modes propagating along the [110] direction. Longitudinal and shear modes with polarization parallel and perpendicular to the [001] direction were generated along the [001] and [110] directions. With respect to the tetragonal symmetry of $(TaSe_4)_2I$ (space group $I422$) the different sound velocity measurements give access to five elastic constants. With the orientation of the available crystals it is not possible to determine C_{13}.

The standard pulse-echo technique was used between 15 and 110 MHz with $LiNbO_3$

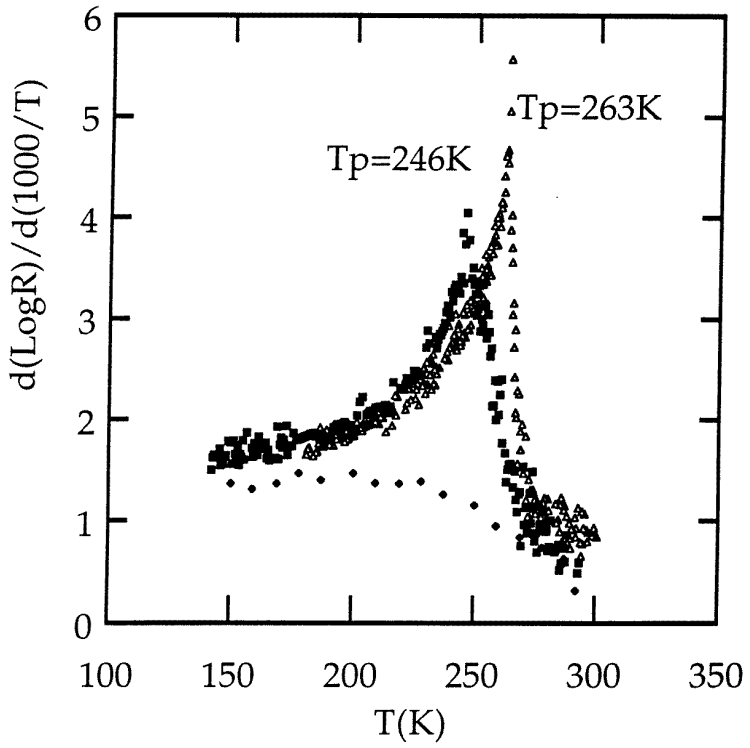

Figure 1. The logarithmic derivative of the electrical resistance as a function of temperature of: pure $(TaSe_4)_2I$, △ (batch B: $T_P = 263$ K); doped $(Ta_{1-x}Nb_xSe_4)_2I$ with $x = 0.2\%$, ■ (batch D: $T_P = 246$ K); and doped $(Ta_{1-x}Nb_xSe_4)_2I$ with $x = 1.2\%$, ● (batch E: $T_P = 200$ K).

transducers. The sound velocity change was measured by phase-coherent detection. Because of the high ultrasonic attenuation at room temperature only one echo is obtained at 15 MHz for the slow shear mode C_{44}, and the inverse of the amplitude of the first echo was measured in decibels and taken as a measure of the attenuation. The lengths of the samples were constant, and fixed at 3 mm.

The thermal expansion coefficient α was measured between 4 and 300 K along the [001] and [110] directions by a capacitance technique [15]. The experimental resolution $\Delta L/L$ was about 10^{-7}.

Electric field effects on the sound velocity of the slow shear mode propagating along the [110] direction and polarized along the [001] direction have been measured on sample A2 with the electric field parallel to the [001] direction. A copper film 5000 Å thick was deposited on the two surfaces perpendicular to the [001] direction in order to obtain good electrical contacts. Care was taken to avoid spurious effects due to sample heating by the electric pulses. We used an experimental procedure similar to that described in [16]. An electric pulse 30 μs wide was applied and its position was adjusted in order to cover completely the travel period of about 5 μs of a selected acoustic echo 1 μs wide. The velocity of the selected echo was measured while the electric pulse was progressively delayed until the selected echo was outside the electric pulse. The field effect on the amplitude of the acoustic echo was too small to be accurately measured.

The specific measurements that we have performed are now listed.

2.1. $(TaSe_4)_2I$ samples

(1) The sound velocity and attenuation of the slow shear mode C_{44} propagating along the [001] direction ($\boldsymbol{q} \parallel \boldsymbol{c}$) with polarization perpendicular to this direction ($\boldsymbol{u} \perp \boldsymbol{c}$), and of the longitudinal mode C_{33} along the $\boldsymbol{c}$-direction have been measured on the same sample, A1 (from batch A). Measurements of the thermal expansion along the $\boldsymbol{c}$ direction have been performed on the same crystal.

(2) The sound velocity of the C_{44}-mode propagating perpendicularly to the [001] direction ($\boldsymbol{q} \perp \boldsymbol{c}$) with polarization along the chain axis ($\boldsymbol{u} \parallel \boldsymbol{c}$) has been measured for sample B (from batch B).

(3) The thermal expansion along the [110] direction was measured for sample C.

2.2. Doped $(Ta_{1-x}Nb_xSe_4)_2I$ samples

(1) The sound velocity and attenuation of the C_{44}-mode propagating along the [110] direction with polarization along the chain axis ($\boldsymbol{u} \parallel \boldsymbol{c}$) were measured for sample D (from batch D: $x = 0.2\%$).

(2) The sound velocity and attenuation of the C_{44}-mode propagating along the [001] direction ($\boldsymbol{q} \parallel \boldsymbol{c}$) with polarization perpendicular to this direction ($\boldsymbol{u} \perp \boldsymbol{c}$), and of the longitudinal mode C_{33} were measured for sample E (from batch E: $x = 1.2\%$).

Table 1. The sound velocity (in (m s^{-1}) and elastic moduli (in units of 10^{10} N m^{-2}) at room temperature.

		Elastic constant	Sound velocity
$(TaSe_4)_2I$			
	C_{11}:	3.94	2500
	C_{33}:	11.5	4260
	C_{44}:	0.128	450
	C_{66}:	1.42	1500
	C_{12}:	1	
$(Ta_{1-x}Nb_xSe_4)_2I$			
	$x = 0.2\%$		
	C_{44}:		465
	$x = 1.2\%$		
	C_{44}:		510

3. Results

The elastic constants were deduced from the sound velocity results and are given for room temperature in table 1; the mass density d is 6.3 g cm^{-3}. The shear constant $C_{44} = dV_{44}^2$ has an unusually small value corresponding to the small sound velocity V_{44} of 450 m s^{-1}. V_{44} exhibits a large anomaly at the Peierls transition. We report a detailed study of the slow shear mode C_{44}.

3.1. The slow shear mode C_{44}

In the tetragonal symmetry ($I422$) of $(TaSe_4)_2I$ the shear mode C_{44} corresponds either to the elastic mode having the wavevector $\boldsymbol{q} \parallel \boldsymbol{c}$ and displacement vector $\boldsymbol{u} \perp \boldsymbol{c}$ or to the elastic

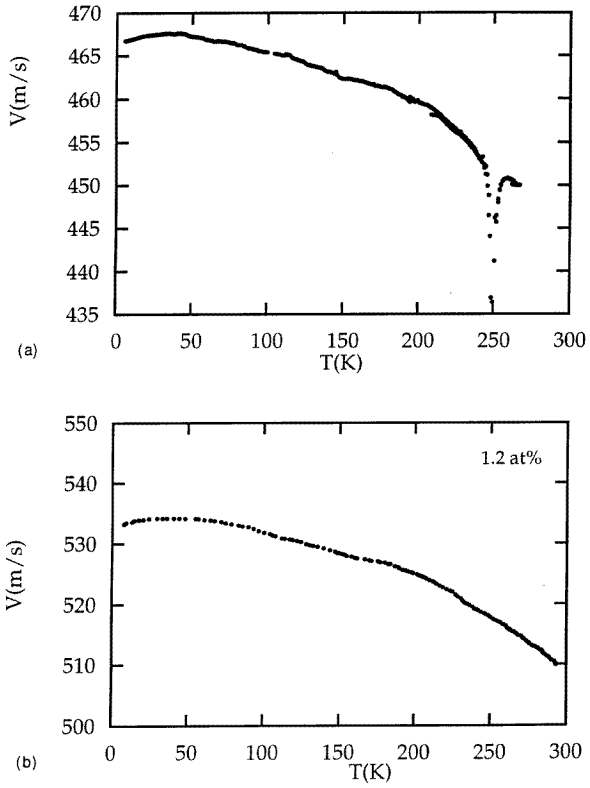

Figure 2. The temperature dependence of the sound velocity V_{44} of the slow shear mode C_{44} (a) with propagation perpendicular to the chain axis $\boldsymbol{c}$ ($\boldsymbol{q} \perp [110]$) and displacement $\boldsymbol{u} \parallel [001]$ at 15 MHz for $(TaSe_4)_2I$ sample B ($T_P = 250$ K) (the solid line has been calculated using equation (2) with the Debye temperature $\theta_D = 124$ K and the Gruneisen parameter $\Gamma_{eff} = 0.45$); (b) with propagation along the chain axis ($\boldsymbol{q} \parallel \boldsymbol{c}$) and displacement $\boldsymbol{u} \perp \boldsymbol{c}$ at 15 MHz for $(Ta_{1-x}Nb_xSe_4)_2I$ sample E ($x = 1.2\%$, $T_P = 200$ K).

mode with $\boldsymbol{q}$ in the basal plane, $\boldsymbol{q} \perp \boldsymbol{c}$ and $\boldsymbol{u} \parallel \boldsymbol{c}$, $\boldsymbol{c}$ being the chain axis. Measurements have been performed with these two configurations; the direction of $\boldsymbol{q}$ in the basal plane was determined by x-ray measurements. Measurements performed with the two polarizations $\boldsymbol{u} \parallel \boldsymbol{c}$ and $\boldsymbol{u} \perp \boldsymbol{c}$ are shown respectively in figures 2 and 3. A large decrease of the V_{44} sound velocity and a sharp peak in the ultrasound attenuation are observed at the Peierls transition T_P for both configurations.

An *anisotropic behaviour* is observed in the sound velocity and attenuation of the slow shear mode C_{44} with the two polarizations $\boldsymbol{u} \perp \boldsymbol{c}$ (figure 3(a)) and $\boldsymbol{u} \parallel \boldsymbol{c}$ (figure 3(b)) measured at the same frequency of 15 MHz for samples A1 and A2 of the same batch ($T_P = 263$ K). The broad and large peak in attenuation at 275 K obtained with $\boldsymbol{q} \parallel \boldsymbol{c}$ and $\boldsymbol{u} \perp \boldsymbol{c}$ is *not observed* for the other configuration $\boldsymbol{q} \parallel [110]$ and $\boldsymbol{u} \parallel \boldsymbol{c}$. At 45 MHz, attenuation at T_P is very high and the acoustic echo vanishes.

The minimum of the sound velocity V_{44} and the sharp peak in attenuation are very sensitive to the niobium content (figure 2(b) and figure 3(b)). There is a similar broadening at T_P in the temperature dependence of C_{44} and in the temperature dependence of the electrical resistance for low Nb doping. For the doped $x = 1.2\%$ sample no sharp peak in

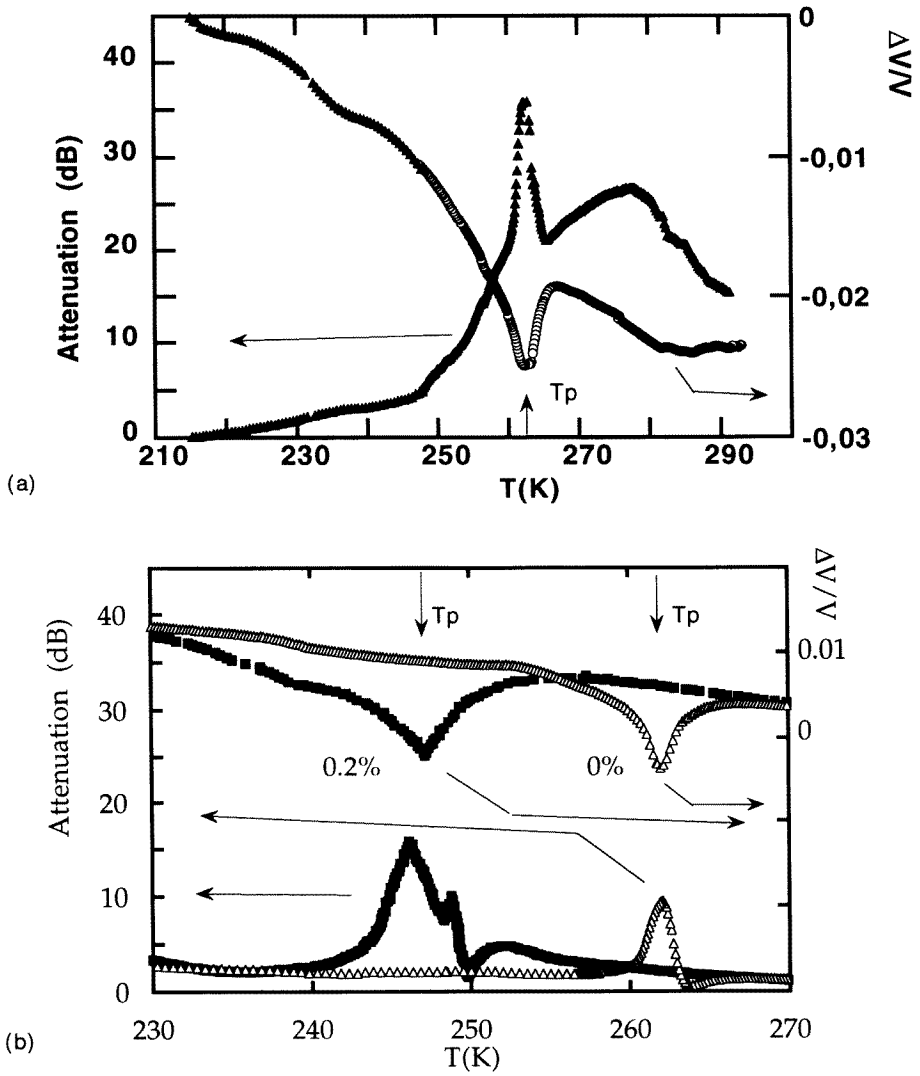

Figure 3. The relative change of the sound velocity $\Delta V/V = V(T) - V(T^*)/V(T^*)$ and relative change in attenuation of the slow shear mode C_{44} (a) with propagation along the $\boldsymbol{c}$-axis ($\boldsymbol{q} \parallel \boldsymbol{c}$) and polarization $\boldsymbol{u} \perp \boldsymbol{c}$ measured at 15 MHz for $(TaSe_4)_2I$ (sample A1, $T_P = 263$ K) (0 dB is normalized to the value at 220 K and $T^* = 210$ K); (b) with propagation along the [110] direction and polarization $\boldsymbol{u} \parallel \boldsymbol{c}$ measured at 15 MHz for $(TaSe_4)_2I$, △ (sample A2, $T_P = 263$ K) and for $(Ta_{1-x}Nb_xSe_4)_2I$ with $x = 0.2\%$, ■ (sample D, $T_P = 246$ K) (0 dB is normalized to the value at 290 K and $T^* = 290$ K).

the electrical derivative (figure 1) and no dip in the sound velocity (figure 2(b)) is observed. Figure 4 shows the comparison between the temperature dependence of the ultrasound attenuation of the pure $(TaSe_4)_2I$ (sample A1) already shown in figure 3(a) with that of $(Ta_{1-x}Nb_xSe_4)_2I$ with $x = 1.2\%$ (sample E) in the same geometry: $\boldsymbol{q} \parallel \boldsymbol{c}$ and $\boldsymbol{u} \perp \boldsymbol{c}$. No peak is measured for the doped sample. Doping smears out the Peierls transition. It should

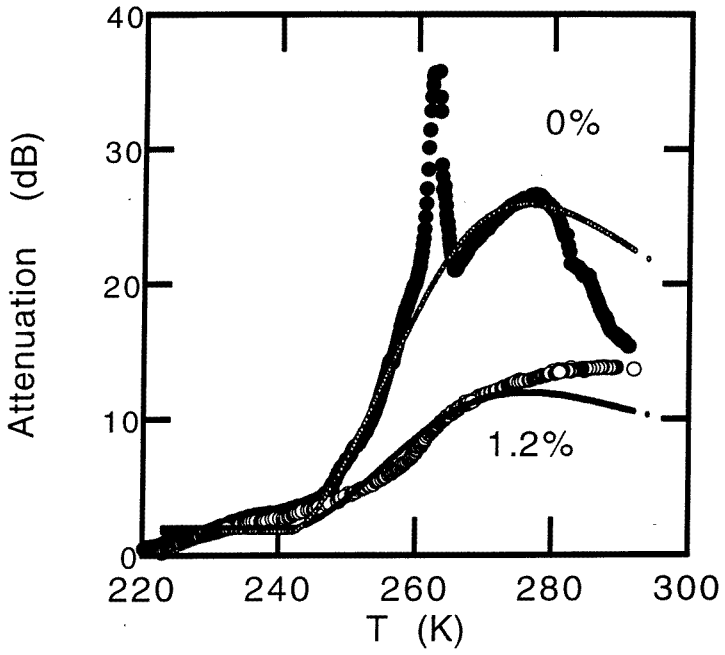

Figure 4. The relative change in attenuation in dB (0 dB is normalized to the value at 220 K) of the shear C_{44}-mode propagating along the chain axis $\boldsymbol{q} \parallel \boldsymbol{c}$ and for $\boldsymbol{u} \perp \boldsymbol{c}$ measured at 15 MHz for $(TaSe_4)_2I$, ● (sample A1, $T_P = 263$ K, as reproduced from figure 1(a)) and for $(Ta_{1-x}Nb_xSe_4)_2I$, ○, with $x = 1.2\%$ (sample E, $T_P = 200$ K). The small points have been calculated using equation (9) with $T_0 = 242$ K and $\tau_0 = 5.7 \times 10^{-9}$ s for samples A1 and E.

also be noted that sound attenuation of the C_{44}-mode at around 270 K as shown in figure 3 for the sample that was 1.2% Nb doped is smaller than the attenuation for pure $(TaSe_4)_2I$.

Careful measurements in the temperature range around the Peierls transition show that the maximum of the attenuation is observed at a temperature T_M lower than the corresponding sound velocity minimum T_m. $T_m - T_M \simeq 0.2$ K for pure samples and $T_m - T_M \simeq 1.2$ K for the sample that was 0.2% doped.

Table 2. Values of the Peierls transition temperature, relaxation time τ ($\tau = \tau_0[1 - T/T_P]^{-\epsilon}$, $\tau_0 = 10^{-12}$ s), and applied voltage V along the $\boldsymbol{c}$-axis.

		Attenuation		
Compounds	Voltage (V)	T_P	T_{Max}	ϵ
$TaSe_4)_2I$		262.3	262.1	1.65
	0.2	—	261.1	3.9
	1	—	261.6	3.4
$(Ta_{1-x}Nb_xSe_4)_2I$, $x = 0.2\%$		247	246	3.8

A similar result has been observed in elastic measurements for the layered dichalcogenides TaS_2 and $NbSe_2$ [17]. It has been interpreted in terms of two processes: one is that of fluctuations of the order parameter and the second is an order parameter relaxation process which contributes only below T_P. The minimum of the sound velocity

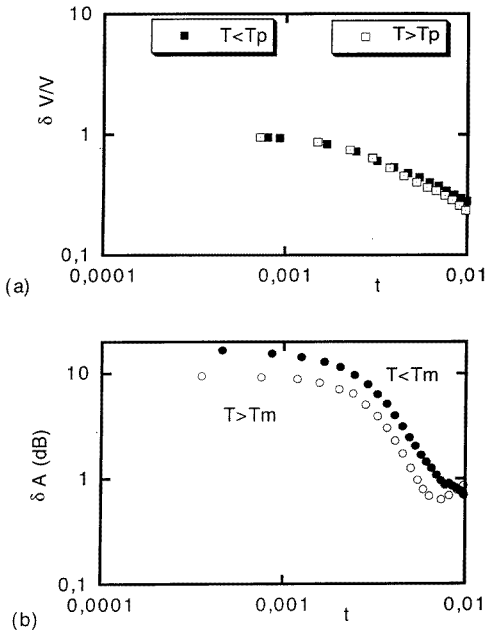

Figure 5. Pure $(TaSe_4)_2I$, sample A2; the transverse mode with $\boldsymbol{q} \parallel \boldsymbol{c}$, $\boldsymbol{u} \perp \boldsymbol{c}$ (figure 3). (a) The temperature dependence of the relative change in the sound velocity $\delta V/V$ (after subtraction of the background contribution) as a function of the reduced temperature $|1 - T/T_P|$ on a logarithmic scale; T_P is the Peierls transition temperature at which V_{44} is minimum. (b) The temperature dependence of the sound attenuation (after subtraction of the background contribution) as a function of the reduced temperature $|1 - T/T_M|$ on a logarithmic scale; T_M is the temperature at which the attenuation takes its maximum value.

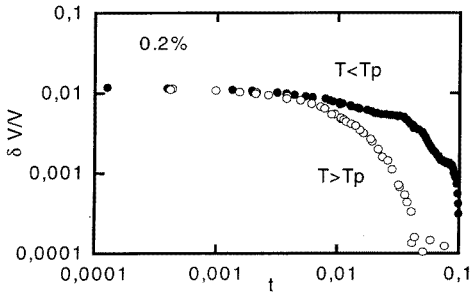

Figure 6. $(Ta_{1-x}Nb_xSe_4)_2I$, $x = 0.2\%$, sample D; the mode with $\boldsymbol{q} \parallel [110]$, $\boldsymbol{u} \parallel \boldsymbol{c}$ (figure 3). The temperature dependence of the relative change in the sound velocity $\delta V/V$ (after subtraction of the background contribution) as a function of the reduced temperature $|1 - T/T_P|$ on a logarithmic scale.

is related to the phase transition temperature T_P. The maximum in attenuation occurs at a temperature T_M for which the matching condition $\omega\tau = 1$ between the sound frequency ω and the relation time τ for the process is fulfilled. Assuming that the relaxation time of the order parameter has a power-law divergence $\tau = \tau_0|T/T_P - 1|^{-\epsilon}$ and using the condition $\omega\tau = 1$ at the maximum, we calculate the relaxation time coefficient $\epsilon \sim 3.8$

with $\tau_0 = 10^{-12}$ s (table 2).

In order to analyse the anomaly found with the mode with $\boldsymbol{q} \parallel [001], \boldsymbol{u} \perp [001]$, we have subtracted the background contribution measured with the sample that was 1.2% doped with the same mode. The relative sound velocity change

$$\frac{\delta V}{V} = \frac{\Delta V}{V}[0\%] - \frac{\Delta V}{V}[1.2\%]$$

and the relative attenuation

$$\delta A = A[0\%] - A[1.2\%]$$

show a large *asymmetric anomaly* around the Peierls transition. A possible origin of the large peak in attenuation above T_P will be analysed in the following discussion (subsection 4.4).

The temperature-dependent background contribution has also been subtracted for the transverse mode with $\boldsymbol{q} \parallel [110]$ and $\boldsymbol{u} \parallel [001]$. The variation with a logarithmic scale of $\delta V/V$ and δA (after subtraction of the background) for pure $(TaSe_4)_2I$ (sample A2) is shown in figure 5(a) and figure 5(b) respectively; $t = |1 - T/T_P|$ in figure 5(a) for $\delta V/V$ and $t = |1 - T/T_M|$ in figure 5(b) for δA. A similar plot for the relative change of the sound velocity $\delta V/V$ is given in figure 6 for $(Ta_{1-x}Nb_xSe_4)_2I$ with $x = 0.2\%$ (sample D). It should be noted that a *symmetric* anomaly for the sound velocity and sound attenuation around the Peierls transition is observed with this mode in pure $(TaSe_4)_2I$. In contrast the sound velocity anomaly is strongly *asymmetric* in its temperature dependence for the $x = 0.2\%$ doped crystal.

3.2. Longitudinal modes

The temperature dependence of the sound velocity and of the ultrasound attenuation of the longitudinal mode C_{33} propagating along the $\boldsymbol{c}$-axis in $(TaSe_4)_2I$ (sample A1, $T_P = 263$ K) is shown in figures 7(a) and 7(b) respectively. The same peak in attenuation above T_P is observed at 275 K in the longitudinal (figure 7(b)) and in the shear mode (figure 3(a)). In figure 8 the temperature dependence of the sound attenuation for the longitudinal mode C_{33} of pure $(TaSe_4)_2I$ and that for sample the that was 1.2% Nb doped is drawn. It is noted that for the sample that was 1.2% doped the attenuation peak of the C_{33}-mode is shifted to a lower temperature: 240 K. Meanwhile for the shear mode this peak has nearly vanished (figure 4).

The elastic constants and sound velocity measured in the present work and in our previous report [14] are listed in table 1.

3.3. Thermal expansion

The temperature dependence of the thermal expansion for $(TaSe_4)_2I$ is shown in figure 9(a). $\alpha_\perp$ has been measured for sample C ($T_P = 245$ K) and $\alpha_\parallel$ for sample B ($T_P = 250$ K). $\alpha_\perp$ exhibits a large anomaly at $T_P = 245$ K which corresponds to the minimum of C_{44} measured for the same crystal. In contrast $\alpha_\parallel$ shows a step ten times smaller within the experimental accuracy.

The background contribution, $\alpha_{\perp background}$, has been empirically determined in the temperature range between 150 and 300 K and the anomalous behaviour around T_P has been extracted and is shown in figure 9(b): $\Delta\alpha = \alpha_\perp - \alpha_{\perp background}$.

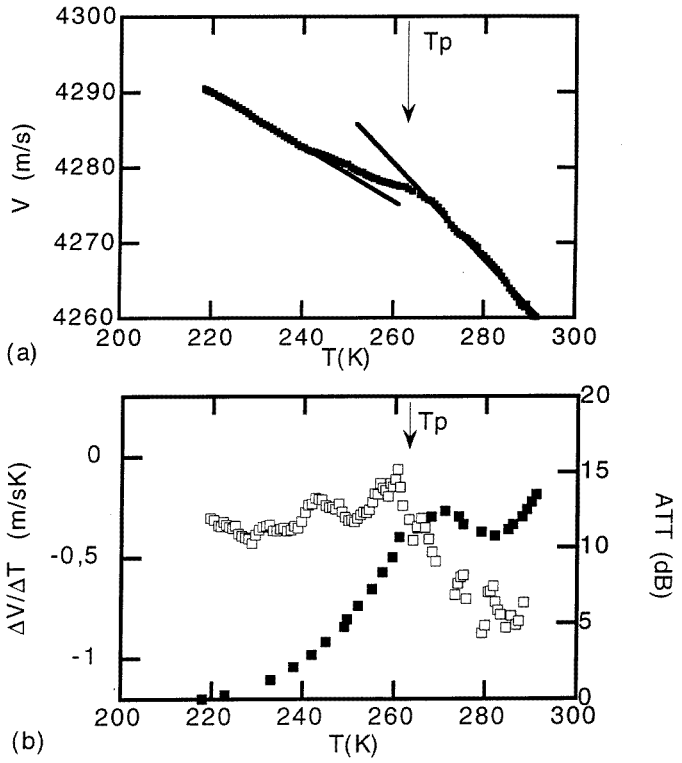

Figure 7. $(TaSe_4)_2I$ (sample A1, $T_P = 263$ K); the longitudinal mode C_{33} propagating along the $\boldsymbol{c}$-axis. (a) The variation of the sound velocity V_{33} with temperature. The solid curves represent the behaviour above and below T_P. (b) The temperature dependence of the variation of the temperature derivative of the sound velocity V_{33}, □, and of the sound attenuation, ■.

4. Discussion

The temperature dependence of the sound velocity V_{44} of the shear C_{44}-mode, as shown in figure 2(a), clearly exhibits three different regimes between 4 and 300 K. A linear temperature dependence is observed between 50 and 200 K. Deviation from this linear behaviour is observed above 200 K. The Peierls transition is characterized by a sharp decrease of V_{44} and a concomitant narrow peak with a large amplitude of the sound attenuation. Above T_P a broad and large peak in the attenuation of the C_{44}-mode is only observed in the configuration with $\boldsymbol{q} \parallel \boldsymbol{c}$ and $\boldsymbol{u} \perp \boldsymbol{c}$ and not that with $\boldsymbol{q} \perp \boldsymbol{c}$ and $\boldsymbol{u} \parallel \boldsymbol{c}$. This same peak in attenuation exists, however, for the longitudinal mode (figure 7(b)). Below 50 K, V_{44} decreases when T is reduced down to 4.2 K. We will now analyse in detail these different behaviours as the anisotropic behaviour of the thermal expansion.

4.1. Softening at the Peierls transition

Elastic anomalies at a Peierls transition can be accounted for by a Landau theory with two order parameters [18, 19]. For the discussion of the interaction between the strain e induced by the elastic wave and the order parameter, we consider the expansion of the free energy in powers of the order parameter and the strain components [19]. The structural

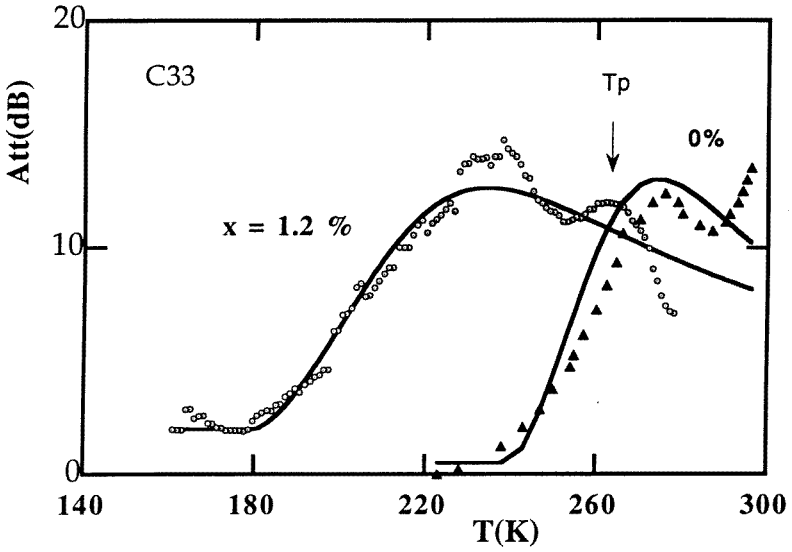

Figure 8. The relative change in attenuation in dB of the longitudinal mode C_{33} ($\boldsymbol{q} \parallel \boldsymbol{u} \parallel \boldsymbol{c}$) measured at 15 MHz for $(TaSe_4)_2I$, ▲ (sample A2, $T_P = 263$ K) and for $(Ta_{1-x}Nb_xSe_4)_2I$, ○, with $x = 1.2\%$ (sample E, $T_P = 200$ K). 0 dB is normalized to the value at 160 K and 220 K respectively. The curves have been calculated using equations (8) and (9) with $T_0 = 242$ K and $\tau_0 = 5.7 \times 10^{-9}$ s (▲) and $T_0 = 180$ K and $\tau_0 = 1.8 \times 10^{-8}$ s (○).

transition of $(TaSe_4)_2I$ at T_P is characterized by a non-zero wavevector associated with the order parameter [9, 10]. It follows that the strains e can only couple with even powers of the order parameter in an incommensurate phase transition [18]. The existence of eight superstructure wavevectors q_s [10] leads to a four components η_i of the order parameter.

The interaction energy F_c is phenomenologically expanded in powers of e and the four components η_i of the order parameter Q, taking into account the $I422$ symmetry:

$$\begin{aligned} F_c = {} & [\lambda_1(e_1 + e_2) + \lambda_2]\left[\eta_1^2 + \eta_2^2 + \eta_3^2 + \eta_4^2\right] \\ & + \mu\left[(e_4 + e_5)(\eta_1^2 - \eta_3^2) + (e_4 - e_5)(\eta_4^2 - \eta_2^2)\right] \\ & + \nu e_6\left[\eta_1^2 - \eta_2^2 + \eta_3^2 - \eta_4^2\right] \end{aligned}$$

and the elastic energy:

$$\begin{aligned} F_e = {} & \frac{1}{2}C_{11}(e_1^2 + e_2^2) + \frac{1}{2}C_{12}e_1e_2 + \frac{1}{2}C_{13}(e_1e_3 + e_2e_3) \\ & + \frac{1}{2}C_{33}e_3^2 + \frac{1}{2}C_{44}(e_4^2 + e_5^2) + \frac{1}{2}C_{66}e_6^2. \end{aligned}$$

The Landau energy F_0 contains the following terms:

$$\begin{aligned} F_0 = {} & \frac{1}{2}A\left[\eta_1^2 + \eta_2^2 + \eta_3^2 + \eta_4^2\right] + \frac{B_0}{4}\left[\eta_1^4 + \eta_2^4 + \eta_3^4 + \eta_4^4\right] \\ & + \frac{B_1}{4}\left[\eta_1^2\eta_3^2 + \eta_2^2\eta_4^2\right] + \frac{B_2}{4}\left[\eta_1^2\eta_2^2 + \eta_2^2\eta_3^2 + \eta_3^2\eta_4^2\right] + \cdots. \end{aligned}$$

For simplicity, we take $\eta_1 = \eta$ and $\eta_2 = \eta_3 = \eta_4 = 0$, and one then obtains the new elastic

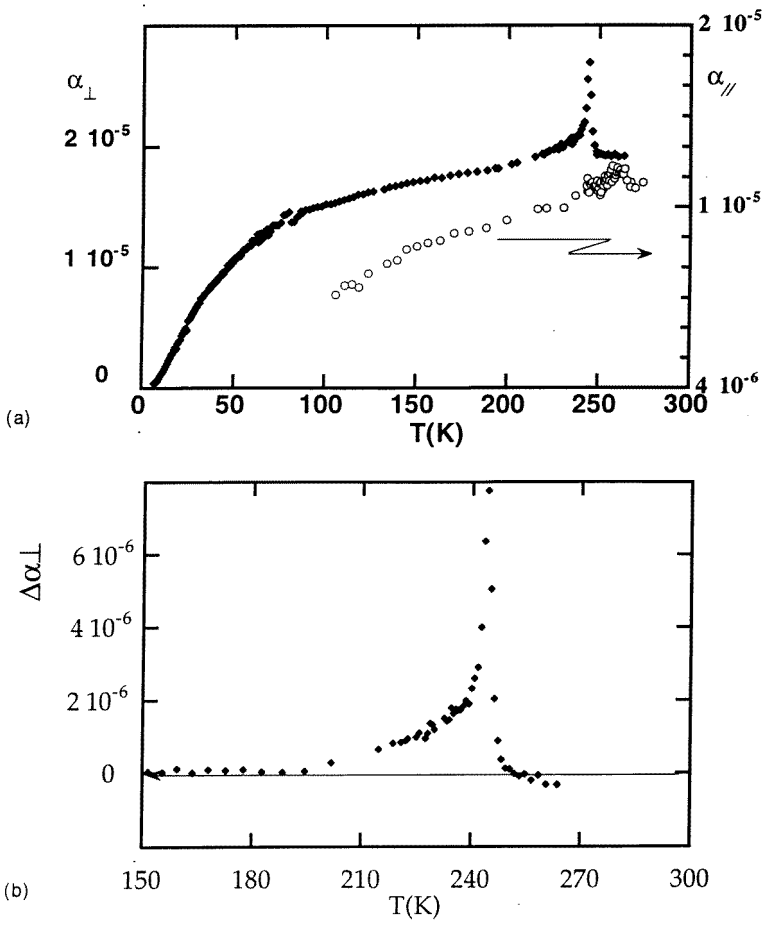

Figure 9. (a) The temperature dependences of the thermal coefficients $\alpha_\perp$ and $\alpha_\parallel$ measured along the [110] and [001] directions respectively for $(TaSe_4)_2I$ (♦: sample C, $T_P = 245$ K; ○: sample A1, $T_P = 263$ K). (b) The temperature dependence of the differential thermal expansion $\Delta\alpha = \alpha_\perp - \alpha_{th}$ (α_{th}, the thermal expansion coefficient, has been calculated using equation (2)) for $(TaSe_4)_2I$, ♦ (sample C, $T_P = 245$ K).

constant C_{44} by minimizing the free energy with respect to e_4 and e_5:

$$C_{44} = C_{44}^0 - \frac{\mu^2}{2B_0}.$$

C_{44}^0 is the background elastic constant. The discontinuity of C_{44} in the mean-field approximation is controlled by the coupling coefficient μ. A similar anomaly is expected for all of the elastic constants. The value of C_{44}^0 is much smaller than the other values (see table 1). This has the result that the largest relative discontinuity at T_P is expected only for C_{44} in the case where $\lambda = \mu = \nu$.

However, critical fluctuations in the order parameter are extremely important in the one-dimensional materials [18, 19, 20, 21]. They are responsible for the large dip in the sound velocity at T_P [18]. The sound velocity V_{44} and thermal expansion coefficient $\alpha_\perp$ along the [110] direction have the same critical behaviour near the Peierls transition (see figure 9(b)

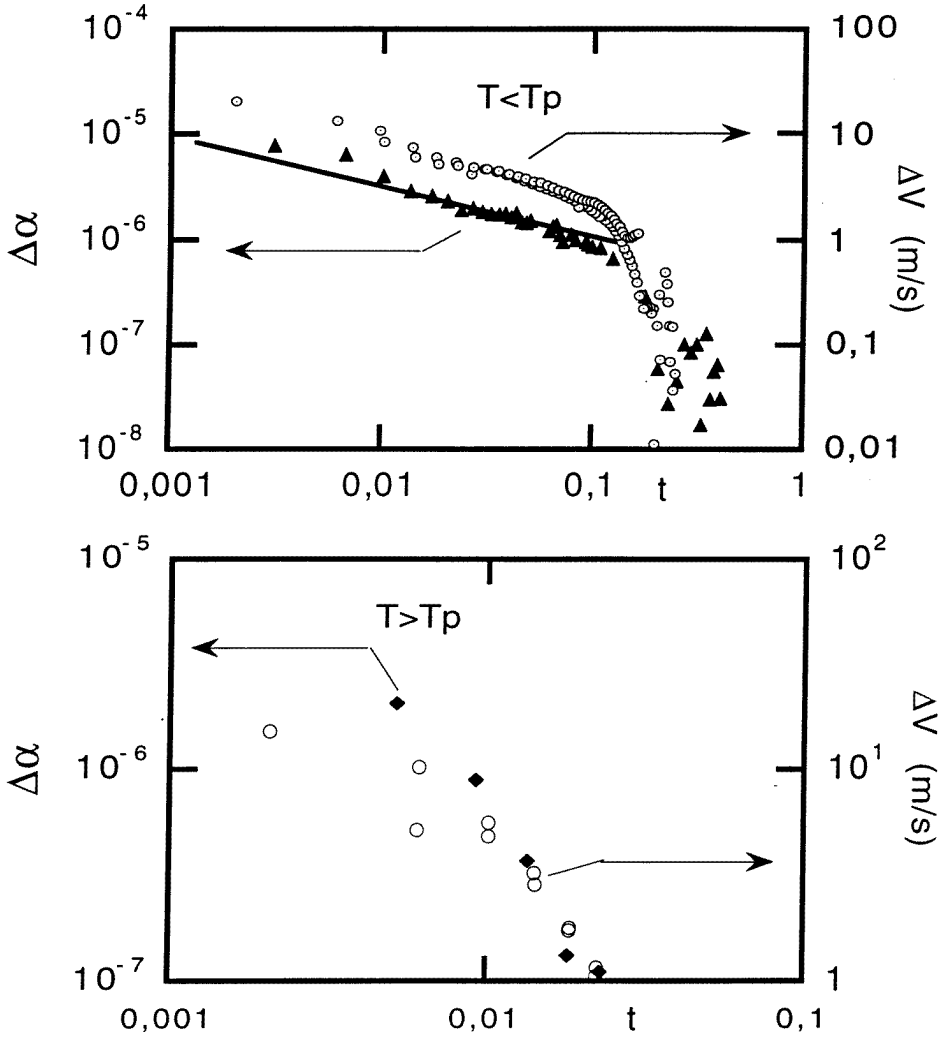

Figure 10. The variation of the relative sound velocity ΔV_{44} ($(TaSe_4)_2I$, sample B) and of the thermal expansion $\Delta\alpha$ ($(TaSe_4)_2I$, sample C) as a function of the reduced temperature $|1 - T/T_P|$ on a logarithmic scale (upper panel) for $T < T_P$ and (lower panel) for $T > T_P$.

and figure 2(a), respectively). In figure 10 the variations of ΔV (for the C_{44}-mode, after subtraction of the background) and $\Delta\alpha_\perp$ are plotted as functions of the reduced temperature $|1 - T/T_P|$ on a logarithmic scale. The same critical exponent of about 0.5 is observed below T_P (figure 10, upper panel) over a large temperature range of about 40 K and the same critical exponent of about 1 is observed above T_P:

$$\Delta V, \Delta\alpha_\perp \cong \left|\frac{T}{T_P} - 1\right|^{-\rho}$$

$$\rho = 0.5 \qquad T < T_P$$

$$\rho \simeq 1 \qquad T > T_P$$

Electro-acoustic effects observed at T_P (see figure 15, later) confirm that the dip in the sound velocity of C_{44} and peak in the attenuation are due to the fluctuations of the CDW order parameter.

4.2. Anharmonicity

The normal behaviour observed in many solids is the decrease of the sound velocity or elastic constant with increasing temperature which can be successfully described by the anharmonicity of the lattice vibrations. The temperature dependence of the sound velocity is related to the Grüneisen parameter. The expression for the temperature dependence of the sound velocity V due to the anharmonic contribution may be written [22] as

$$V(T) - V(T=0) = -\frac{1}{2}\frac{\Gamma_{eff}^2 C(T)}{dV(T=0)}T \tag{1}$$

where Γ_{eff} is the effective Grüneisen parameter which describes the anharmonic coupling of the external strain to the thermal phonon modes and $C(T)$ is the specific heat. At high temperatures, $T \geqslant \theta_D$, θ_D being the Debye temperature, a constant value of Γ_{eff} in equation (1) gives a linear temperature dependence of the sound velocity.

From the linear temperature dependence observed between 100 and 200 K in figure 2(a) the value $\Gamma_{eff} \simeq 0.45$ is deduced for the shear C_{44}-mode. C_T has been calculated with a Debye specific heat having a Debye temperature of $\theta_D \simeq 124$ K as deduced from the low-temperature specific heat measurements [23] and an atom number $N = 11$. However, the constant value of Γ_{eff} in equation (1) cannot explain the decrease of the sound velocity at the lowest temperature (figure 2(a)). A tentative explanation will be given below.

The temperature dependence of the thermal expansion in solids is also related to the anharmonic effects. The thermal expansion coefficient is related to the thermal Grüneisen parameter γ:

$$\alpha \simeq \frac{1}{3}\frac{C(T)\gamma}{B} \tag{2}$$

where $C(T)$ is the specific heat and B the bulk modulus. Taking $B \simeq 10^{11}$ N m^{-2} and the Debye specific heat $C(T)$ with $\theta_D \simeq 124$ K, γ can be estimated to be $\sim$3 in the temperature range around 100 K.

4.3. The thermal expansion in the vicinity of T_P

Anomalies in elastic and thermal properties at second-order phase transitions are related by Ehrenfest relations [24]:

$$\Delta\alpha_i = -(\Delta C_P/T_P)\frac{\mathrm{d}T_P}{\mathrm{d}\sigma_i} \tag{3}$$

$$\Delta C_{ii} = -C_{ii}(\Delta C_P/T_P)\left(\frac{\mathrm{d}T_P}{\mathrm{d}\sigma_i}\right)^2 \tag{4}$$

where C_P is the specific heat, α_i the thermal expansivity, C_{ii} the isothermal longitudinal elastic constant and $\mathrm{d}T_P/\mathrm{d}\sigma_i$ the stress dependence of T_P in the ith direction. For $(TaSe_4)_2I$, no specific heat measurement around T_P has been reported and the specific heat discontinuity ΔC_P at T_P is not known.

Longitudinal elastic constants are compared to the thermal expansion. The magnitudes of the step of the thermal expansion coefficient $\Delta\alpha_\parallel \simeq 10^{-6}$ K^{-1} and $\Delta\alpha_\perp \simeq 8\times10^{-6}$ K^{-1} are measured at T_P as shown in figure 9(a).

A pressure dependence $dT_P/dp \simeq 1$ K kbar^{-1} has been measured by Forro *et al* [25]. Tetragonal symmetry leads to the relation

$$dT_P/dp = 2\ dT_P/d\sigma_{110} + \ dT_P/d\sigma_{001}. \tag{5}$$

Equations (3) and (5) give

$$dT_P/d\sigma_{110} \simeq 0.48 \text{ K kbar}^{-1} \qquad dT_P/d\sigma_{001} \simeq 0.06 \text{ K kbar}^{-1}.$$

The anisotropic behaviour of the thermal expansion of $(TaSe_4)_2I$ is related to the anisotropic stress dependence $dT_P/d\sigma$. Equations (3) and (4) give

$$\frac{\Delta C_{ii}}{C_{ii}^2} = \Delta\alpha_{ii}\ \frac{dT_P}{d\sigma_i}.$$

The very small value of $dT_P/d\sigma_{001}$ leads to a discontinuity, $\Delta C_{33}/C_{33} \simeq 10^{-4}$, at T_P. This value is in agreement with the experimental results, as shown in figure 7(a).

4.4. Low-temperature behaviour of the C_{44}-mode

From figure 2(a) it can be seen that at low temperatures below 50 K, the sound velocity V_{44} does not follow equation (1) and decreases when T is reduced. This decrease of the sound velocity of the slow shear modes has been observed for all of the pure and doped $(TaSe_4)_2I$ samples.

The same slow shear mode C_{44} has been measured for $(NbSe_4)_3I$. $(NbSe_4)_3I$ is a quasi-one-dimensional compound with a structure very similar to that of $(TaSe_4)_2I$ but which does not undergo a Peierls transition. Low-temperature anomalies measured in $(TaSe_4)_2I$ were absent in $(NbSe_4)_3I$ [23].

Similarly no anomalous behaviour in the temperature variation of V_{44} is observed in $(NbSe_4)_3I$ as shown in figure 11(a). The increase of the sound velocity with decreasing temperature follows equation (1) with a constant Grüneisen parameter $\Gamma_{eff} \simeq 1.7$. In the same figure, figure 11(a), the relative variation of V_{44} normalized at $T = 80$ K is shown for pure $(TaSe_4)_2I$ (sample A1) and for $(Ta_{1-x}Nb_xSe_4)_2I$ with $x = 0.2\%$ (sample D) and $x = 1.2\%$ (sample E). It can be noted that at $T = 4.2$ K, the sound velocity V_{44} is equal to that at 80 K. Figure 11(b) shows the frequency dependence of the attenuation of sample D in the low-T range.

Assuming the validity of equation (1) to extend to the lowest temperatures, an effective Grüneisen parameter Γ_{eff} can be calculated at each temperature. For the shear mode of $(TaSe_4)_2I$, Γ_{eff} increases from 0.45 to 20 when T decreases from 100 K to 4.2 K as shown in figure 12(a).

In equation (1) one further term must be taken into account to explain this divergence of Γ_{eff}. Reformulation of the temperature dependence of the sound velocity must be undertaken when anisotropy is included [26, 27]:

$$V(T) - V(T=0) = -\frac{1}{2dV}\left[C(T)\Gamma^2 - u\ \frac{\partial\Gamma}{\partial\epsilon}\right] \tag{6}$$

where u is the phonon density energy and $\partial\Gamma/\partial\epsilon$ is the strain derivative of the Grüneisen parameter. The term $u\ \partial\Gamma/\partial\epsilon$ indicates averaging over the phonon modes weighted by the mode energies. The negative temperature dependence of the sound velocity requires the second term $u\ \partial\Gamma/\partial\epsilon$ in equation (6) to be the largest. This implies that the fourth-order anharmonicity is important for the slow shear mode C_{44}. The linear temperature dependence observed between 5 and 20 K indicates that the phonon density u in equation (1) must

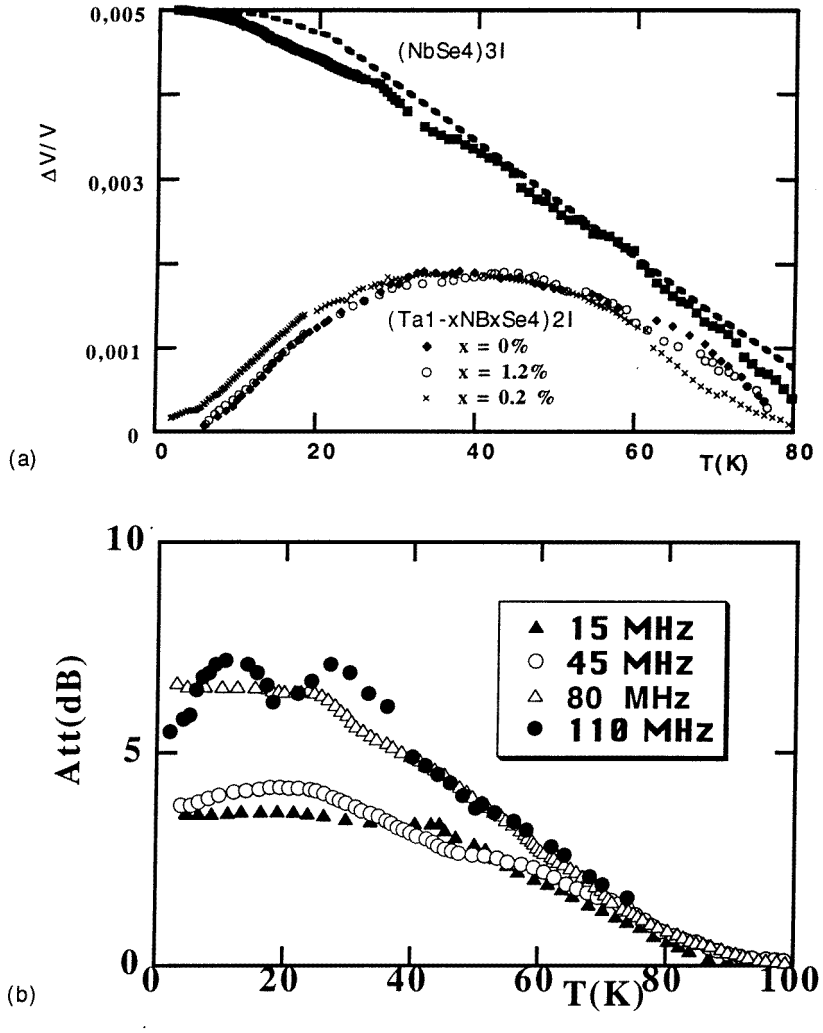

Figure 11. (a) The relative change of the sound velocity of the slow shear C_{44}-mode normalized at 80 K for pure $(NbSe_4)_3I$ and doped $(TaSe_4)_2I$ (the dashed line was obtained by calculation using equation (1) with $\Gamma_{eff} = 1.7$. (b) The relative attenuation of the slow shear mode in $(Ta_{1-x}NbSe_4)_2I$ with $x = 0.2\%$ (sample D) measured at different frequencies.

increase linearly with temperature over the same temperature range, assuming a constant $\partial\Gamma/\partial\epsilon$-term.

A low-lying strongly dispersive transverse acoustic mode has been indicated by neutron experiments [10]. This mode is characterized by a constant frequency $\omega_m/2\pi = 0.15$ THz over a large part of the Brillouin zone. ω_m corresponds to a temperature $\theta_E \simeq 7$ K; $\hbar\omega_m = k\theta_E$. The Einstein phonon density energy u in equation (1) with $\theta_E = 7$ K describes a linear temperature decrease of the sound velocity with $\partial\Gamma/\partial\epsilon \simeq 0.05$. Thus, the anomalous increase of the elastic constant C_{44} or sound velocity v_{44} below 20 K is due to the main contribution of the low-lying transverse mode.

An anomalous behaviour of the ultrasonic attenuation is observed below 50 K. The

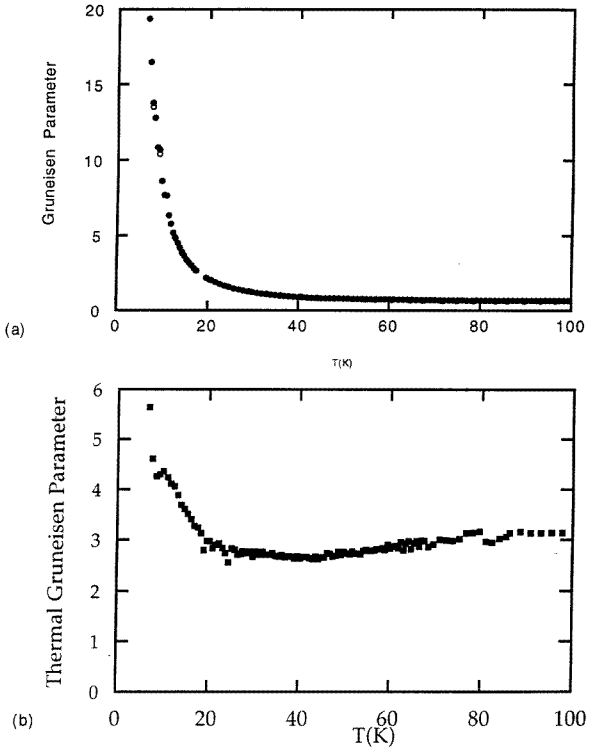

Figure 12. (a) The temperature dependence of the effective Grüneisen parameter Γ_{eff} deduced from the sound velocity of the slow shear modes (figure 2(a)) using equation (1); 0% (●) and 1.2% (○). (b) The temperature dependence of the thermal Grüneisen parameter deduced from the thermal expansion coefficient $\alpha_\perp$ (figure 9) using equation (2).

attenuation observed in crystalline solids at low temperatures is attributed to the interaction between the ultrasonic wave and the lattice vibrations, and in general the attenuation decreases with decreasing temperature [22]. An opposite behaviour is observed in pure and doped $(TaSe_4)_2I$ (figure 11(b)). Measurements performed at different frequencies on the sample that was 0.2% Nb doped are only reported in figure 11(b); similar results have been obtained for pure samples and samples that were 1.2% Nb doped.

The anomalous behaviours of both the sound velocity and the attenuation are related to the low-lying and strongly dispersive transverse acoustic mode of $(TaSe_4)_2I$.

Similarly the transverse thermal expansion does not follow equation (2) at low temperatures. From the measured $\alpha_\perp$ and the calculated $C(T)$ at low T, γ is shown to increase from 3 to 6 below 20 K. The temperature variation of the thermal Grüneisen parameter γ is plotted in figure 12(b). Both ultrasound and thermal expansion measurements show the same anomalous behaviour below 20 K.

4.5. The sound attenuation peak above T_P

The large peaks in the sound attenuation of the C_{44}-mode—but only with the propagation along the chain axis $\boldsymbol{q} \parallel \boldsymbol{c}$ and $\boldsymbol{u} \perp \boldsymbol{c}$—and of the longitudinal mode C_{33} ($\boldsymbol{q} \parallel \boldsymbol{u} \parallel \boldsymbol{c}$), observed at around 275 K for $(TaSe_4)_2I$ at 15 MHz and 80 MHz, have been analysed as

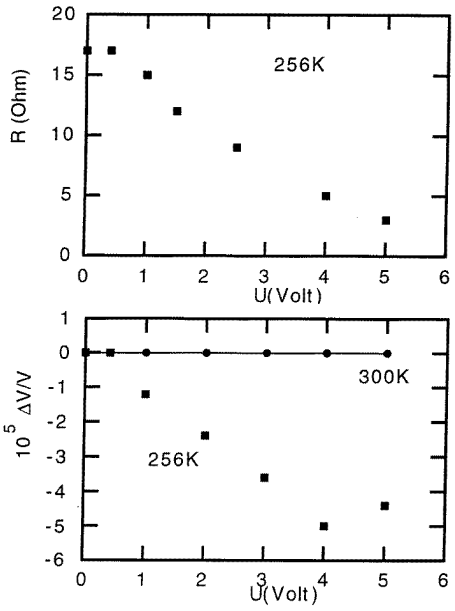

Figure 13. $(TaSe_4)_2I$, sample A2. The electrical resistance as a function of the voltage, and the voltage dependence of the sound velocity of the C_{44}-mode with $\boldsymbol{q} \parallel [110]$, $\boldsymbol{u} \parallel [001]$.

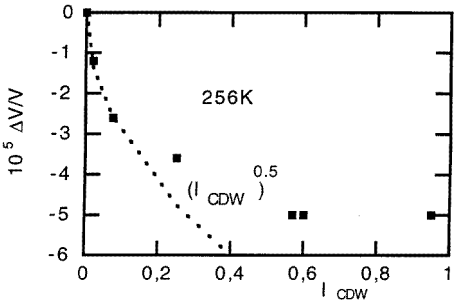

Figure 14. The variation of the sound velocity in the non-linear state as a function of the CDW current.

resulting from a relaxation process characterized by one relaxation time τ. Thus, the sound velocity and the attenuation A are related to the measurement frequency ω and time constant by

$$V(\omega) = V(\infty) - \frac{V(\infty) - V(0)}{1 + (\omega\tau)^2} \tag{7}$$

and

$$A = \frac{V(\infty)^2 - V(0)^2}{2V^3(0)} \frac{\omega^2\tau}{1 + (\omega\tau)^2} = \frac{F}{2dV^3(0)} \frac{\omega^2\tau}{1 + (\omega\tau)^2} \tag{8}$$

where F is the relaxation strength. We first tried to fit the variation of the attenuation peak in C_{44} (figure 4) and in C_{33} (figure 8) to an activated behaviour for τ such as

$$\tau = \tau_0 \exp(T^*/T).$$

Relatively good fits were obtained with an activation energy $T^* \simeq 4500$ K and $\tau_0 \simeq 10^{-16}$ s. This value of 4500 K is much larger than that the Peierls gap, estimated to be 3000 K [4]. Then we tried a power law for τ, given by

$$\tau = \tau_0 \left[\frac{T_0}{T - T_0} \right]^{\epsilon}. \tag{9}$$

The best fits yield a value of $\epsilon = 1.5$. Using equations (8) and (9), the peak in the sound attenuation in C_{44} (the small points in figure 4) can be described with $\tau_0 = 5.7 \times 10^{-9}$ s and $T_0 = 242$ K. The same parameters give a satisfactory fit for the attenuation peak in C_{33} (the solid line in figure 8); thus the anisotropic relaxation strength can be estimated:

$$F_{11} \simeq F_{33} \simeq 10^9 \text{ N m}^{-2}$$

$F_{44}(\boldsymbol{q} \parallel c, \boldsymbol{u} \perp \boldsymbol{c}) \simeq 2 \times 10^7$ N m^{-2}

$F_{44}(\boldsymbol{q} \parallel [110], \boldsymbol{u} \parallel \boldsymbol{c}) \simeq 0.$

In doped $(Ta_{1-x}Nb_xSe_4)_2I$ with $x = 1.2\%$ the small attenuation peak of C_{44} observed at around 230 K can be fitted with a larger value of $\tau_0 = 1.8 \times 10^{-8}$ s and $T_0 = 180$ K (the small points in figure 4) and $\tau_0 = 5.7 \times 10^{-9}$ s and $T_0 = 242$ K for the C_{33}-mode (figure 8).

These measurements show that there is a critical slowing down of relaxing entities which are coupled to the applied elastic wave over a large temperature range around T_P. The relaxation time τ for this process diverges at a temperature T_0 roughly 20 K smaller than T_P. Both temperatures, T_P and T_0, are very sensitive to the Nb doping. It is important to note that the relaxing entities are not coupled to the slow shear C_{44}-mode propagating along the [110] direction with the polarization along the $\boldsymbol{c}$-axis.

The microscopic nature of the relaxing entities cannot be deduced from these ultrasonic measurements alone. This anelastic relaxation process [28] can be related to structural instabilities which already occur above T_P. Strongly correlated fluctuations have been observed above T_P ($T_P + 30$ K) in neutron scattering experiments. The CDW-modulated structure at the Peierls transition implies several $\boldsymbol{q}$-states belonging to distinct domains. We believe that the lattice distortions with various effective orientations are responsible for the relaxation behaviour observed at around T_P.

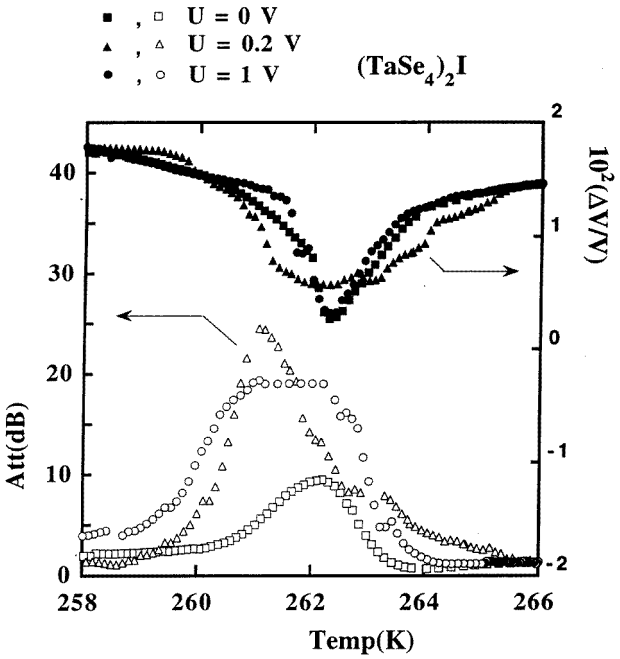

Figure 15. The sound velocity and attenuation of the shear mode C_{44} with $\boldsymbol{q} \parallel [110]$ and $\boldsymbol{u} \parallel [001]$ measured for different values of the electric field applied along the $\boldsymbol{c}$-axis (the U-threshold is at 258 K = 0.5 V) for $(TaSe_4)_2I$ (sample A2).

Relaxation can be due to the stress-induced ordering among preferred orientations of the distortion domains. Relaxation occurs because of the redistribution of entities among sites that are initially inequivalent but which become inequivalent in the presence of the mechanical field [28].

4.6. Electro-acoustic effects

$(TaSe_4)_2I$, like many other quasi-one-dimensional charge-density-wave conductors, exhibits non-linear transport properties below T_P due to the sliding CDW when a voltage higher than a threshold value is applied [1]. Electro-acoustic effects have been studied using the vibrating-reed technique [29]. Hereafter we describe the effect of an applied voltage on the sound velocity of the slow shear mode. We also show that the attenuation peak near T_P is strongly affected if the sample is cooled through T_P under an electric field.

4.6.1. Below T_P. The electric field effect on the sound velocity of the slow shear mode with $\boldsymbol{q} \parallel [110]$, $\boldsymbol{u} \parallel [001]$ (sample A2, $T_P = 263$ K) is shown in figure 13. The voltage U is applied over a distance of 3 mm. The threshold voltage U_T is defined as the voltage at which the electric resistance starts to deviate from the constant ohmic value R_0 [1]. U_T has been shown to increase exponentially when the temperature decreases, and consequently we have only performed field-effect measurements at around 250 K. It can be seen that for $U = 10\,U_T$ the decrease of the sound velocity is $\Delta V/V \simeq 5 \times 10^{-5}$. The charge-density-wave current I_{CDW} was calculated using the relation $I_{CDW} = I - U/R_0$, where I is the total current. The decrease of $\Delta V/V$ follows the $I_{CDW}^{0.5}$-law for small I_{CDW} and saturates at high values as shown in figure 14. A similar behaviour has been found for the Young modulus [12] and shear modulus [29]. The present effects measured at high frequency (15 MHz) are two orders of magnitude smaller than those measured in the kHz frequency range. This indicates that electric field effects in $(TaSe_4)_2I$ follow a frequency dependence $\simeq f^{-1/2}$ which can be compared to the $f^{-3/4}$-law observed for TaS_3 [29].

4.6.2. Electric field effects around the Peierls transition. Measurements of the sound velocity of the slow shear mode with $\boldsymbol{q} \parallel [110]$, $\boldsymbol{u} \parallel [001]$ have been made on cooling through T_P with an applied electric field along the $\boldsymbol{c}$-axis. The dip in the sound velocity and attenuation are sensitive to the applied electric field (figure 15). A large increase of the attenuation is observed with a small applied voltage of 0.2 V. Furthermore the maximum of the attenuation is shifted to lower temperatures. The relaxation rate τ^{-1} depends on the electric field. The condition $\omega\tau = 1$ at T_M with $\tau = \tau_0\,|(T/T_P) - 1|^{-\epsilon}$ leads to the value of the critical exponent ϵ (table 2). The observed electric field effects on the elastic constant C_{44} are thus similar to the effects of doping by Nb.

5. Conclusions

A large dip in the sound velocity of the slow shear mode with a large peak in attenuation are observed at the Peierls transition. A symmetric anomaly is reported for the mode with $\boldsymbol{q} \parallel [110]$, $\boldsymbol{u} \parallel [001]$; meanwhile an asymmetric anomaly is observed for the mode with $\boldsymbol{q} \parallel [001]$, $\boldsymbol{u} \perp [001]$. Fluctuations in the CDW order parameter are responsible for the dip of the sound velocity. The same critical behaviour $[T/T_P - 1]^{-\rho} \simeq 1$ below T_P and above T_P respectively is observed in the temperature dependence of the sound velocity and the thermal expansion coefficients.

An anomalous decrease of the sound velocity of the slow shear mode is reported below 40 K and attributed to the flat dispersion of the slow shear acoustic mode whose characteristic temperature is 7 K. An anomalous behaviour of the thermal Grüneisen parameter deduced from the thermal expansion measurements is shown below 20 K and could be attributed to the same origin. Finally, electro-acoustic effects with transverse acoustic waves are consistent with recent theoretical predictions [30].

References

[1] For a review see
Monceau P 1985 *Electric Properties of Inorganic Quasi-One-Dimensional Materials* Part II, ed P Monceau (Dordrecht: Reidel) p 139; 1989 *Charge Density Waves in Solids (Modern Problems in Condensed Matter Sciences)* ed L P Gork'ov and G Grüner (Amsterdam: North-Holland); 1993 *Electronic Crystals 'ECRYS 93', J. Physique Coll.* **4** C2 3

[2] Gressier P, Whangbo M, Meerschaut A and Rouxel J 1984 *Inorg. Chem.* **23** 1221

[3] Gressier P, Meerschaut A, Guemas L, Rouxel J and Monceau P 1984 *J. Solid State Chem.* **51** 141

[4] Wang Z Z, Saint-Lager M C, Monceau P, Renard M, Gressier P, Meerschaut A, Guemas L and Rouxel J 1983 *Solid State Commun.* **46** 325

[5] Maki K, Kaiser M, Zettl A and Grüner G 1983 *Solid State Commun.* **46** 497

[6] Roucau C, Ayroles R, Gressier P and Meerschaut A 1984 *J. Phys. C: Solid State Phys.* **17** 2993

[7] Fujishita H, Sato S and Hoshino S 1985 *J. Phys. C: Solid State Phys.* **18** 1105

[8] Lee K B, Davidov D and Heeger A J 1985 *Solid State Commun.* **54** 673

[9] Fujishita H, Shapiro S M, Sato M and Hoshino S 1986 *J. Phys. C: Solid State Phys.* **19** 3049

[10] Lorenzo J E, Currat R, Monceau P, Hennion B and Levy F 1993 *Phys. Rev.* B **47** 10 116
Lorenzo J E 1992 *Thesis* Grenoble University

[11] Sugai S, Sato M and Kurihara S 1985 *Phys. Rev.* B **32** 6809

[12] Suzuki A, Mizubayashi H and Okuda S 1988 *J. Phys. Soc. Japan* **57** 4322

[13] Salva H, Ghilarducci A, Monceau P, Levy G, D'Anna G and Benoit W 1995 *Solid State Commun.* **94** 401

[14] Saint-Paul M, Monceau P and Levy F 1988 *Solid State Commun.* **67** 581

[15] de Visser A, Franse J J M and Menovsky A 1985 *J. Phys. F: Met. Phys.* **15** L53

[16] Jericho M H and Simpson A M 1986 *Phys. Rev.* B **34** 1116

[17] Barmetz M, Testardi L R and Di Salvo F J 1975 *Phys. Rev.* B **12** 4367

[18] Rehwald W 1973 *Adv. Phys.* **22** 721

[19] Aronovitz J A, Gilbart P and Mozurkewich G 1990 *Phys. Rev. Lett.* **64** 2799

[20] McKenzie R H 1995 *Phys. Rev.* B **51** 6249

[21] Brill J W, Chang M, Kuo Y K, Zhan X, Figueroa E and Mozurkewich G 1995 *Phys. Rev. Lett.* **74** 1182

[22] Maris H J 1971 *Physical Acoustics* vol 8, ed W P Mason (New York: Academic) p 279

[23] Biljaković K, Lasjaunias J C, Zougmor F, Monceau P, Levy F, Bernard L and Currat R 1986 *Phys. Rev. Lett.* **57** 1907

[24] Testardi L R 1975 *Phys. Rev.* B **12** 3849

[25] Forro L, Mutka H, Bouffard S, Morillo J and Janossy A 1985 *Charge Density Waves in Solids (Springer Lectures Notes in Physics 217)* (Berlin: Springer) p 361

[26] Garber J A and Granato A V 1975 *Phys. Rev.* B **11** 3990

[27] Nava R and Oentrich R 1995 *J. Phys. Chem. Solids* **56** 1077

[28] Nowick A S and Berry B S 1972 *Anelastic Relaxation in Crystalline Solids* (New York: Academic)

[29] Xiang X D and Brill J W 1989 *Phys. Rev. Lett.* **63** 1853

[30] Virosztek A and Maki K 1995 *Synth. Met.* **70** 1283